Springer

KSME

Journal of Mechanical Science and Technology 24 (4) (2010) 909~921
www.springerlink.com/content/1738-494x
DOI 10.1007/s12206-010-0209-7

Modeling of aluminum particle combustion with emphasis on the oxide effects and variable transport properties †

Heesung Yang and Woongsup Yoon*

School of Mechanical Engineering, Yonsei University, Seoul, 120-749, Korea

(Manuscript Received July 27, 2009; Revised January 18, 2010; Accepted January 20, 2010)

Abstract

A simplified analytical modeling of single aluminum particle combustion was conducted. Ignition and quasi-steady combustion (QSC) were separately formulated and integrated. Both the heat transfer from the hot ambient gas and the enthalpy of heterogeneous surface reaction (HSR) served to cause the particle ignition. Conservation equations were solved for QSC parameters in conjunction with conserved scalar formulation and Shvab-Zeldovich function. Limit temperature postulate was formulated by a sink term pertinent to the dissociation of the aluminum oxide near the flame zone. Effective latent heat of vaporization was modified for the thermal radiation. Ignition and QSC of the aluminum particle were predicted and discussed with emphasis on the effect of the aluminum oxide and variable properties. The model was validated with the experiments regarding ignition delay time, burning rate, residue particle size, flame temperature, QSC duration, and stand-off distance of the envelop flame. Agreement was satisfactory and the prediction errors were limited within 10%.

Keywords: Aluminum particle combustion; Heterogeneous surface reaction; Oxide deposition; Oxide smoke effect

1. Introduction

An aluminum particle introduced into high-temperature oxidizer gas experiences the stages of heating, ignition and quasi-steady burning in sequence. This profile of the aluminum particle combustion is similar to the liquid droplet burning, but largely altered due to the presence of the aluminum oxide, an alumina. Ignition delay due to the initial oxide film, deposition of oxide product on the liquid aluminum, and residue oxide particle are notable features [1, 2].

Fig. 1(a) illustrates the sequence of aluminum particle ignition. Either naturally or artificially formed oxide film initially covers the aluminum core. Convective and radiative heat transfer from the hot ambient gas raises the particle temperature, and then the aluminum core inside the solid-phase nonreactive and passivative oxide film begins to melt in advance because the melting temperature of the aluminum oxide is higher than that of the aluminum. Unlike the liquid droplet ignition, the solid oxide film blocks the liquid aluminum from the penetration of the oxidizer hence prevents the particle from its ignition. The oxide film is in a solid-state but its phase transits from amorphous to alpha-state as the particle temperature rises. This phase transition in the solid state increases the density of the aluminum oxide and causes the local exposure of surface of aluminum core to the oxidizer. At these ruptured regions, an exothermic reaction which is called 'Heterogeneous Surface Reaction (HSR) occurs between the liquid aluminum and the gaseous oxidizer [3] and the HSR serves as a primary heat source for ignition [4]. As the particle temperature rises further, the HSR is activated and the aluminum oxide reaches its melting temperature (~2200K). The molten alumina coheres on the liquid aluminum surface and forms an 'oxide cap' in a bulged shape owing to its higher surface tension. The oxide cap grows during quasi-steady combustion period as the reaction product diffuses inward and condenses, and the particle burning ends with the formation of a residue particle (Fig. 1(b)). Because the aluminum oxide continues to condense onto the oxide cap, the inward diffusion of reaction product continues with no radial changes in the concentration gradient of the gaseous product. Effective surface area of the liquid aluminum is reduced by the oxide cap, and violent surface gas ejections and asymmetric combustion may occur [5, 6]. Concurrent with the oxide cap growth, oxide smoke effect [1] occurs. Here, part of the gaseous aluminum oxide diffuses outward and condenses to liquid in the vicinity of the outer flame zone. Endothermic dissociation reaction occurs and limits the flame temperature to the dissociation temperature of aluminum oxide (limit temperature postulate [1]).

† This paper was recommended for publication in revised form by Associate Editor Ohchae Kwon
*Corresponding author. Tel.: +82 2 2123 4812, Fax.: +82 2 312 2159
E-mail address: wsyoon@yonsei.ac.kr

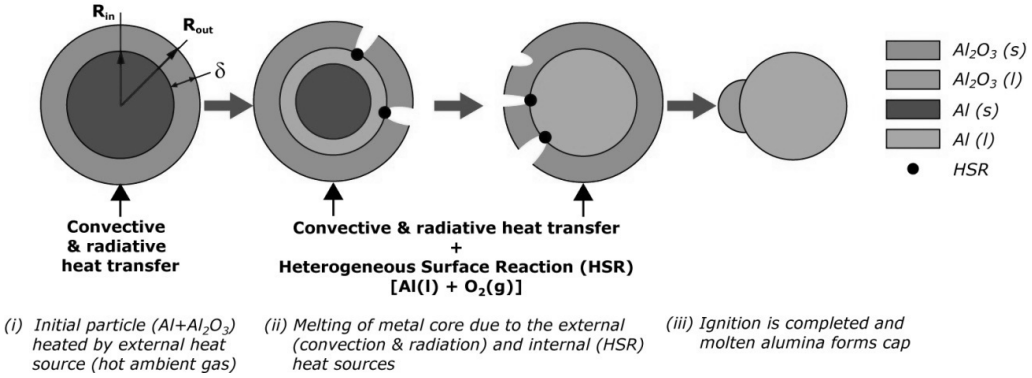

(a) Schematic for ignition stage; from initial particle with oxide film to oxide cap formation with heat sources

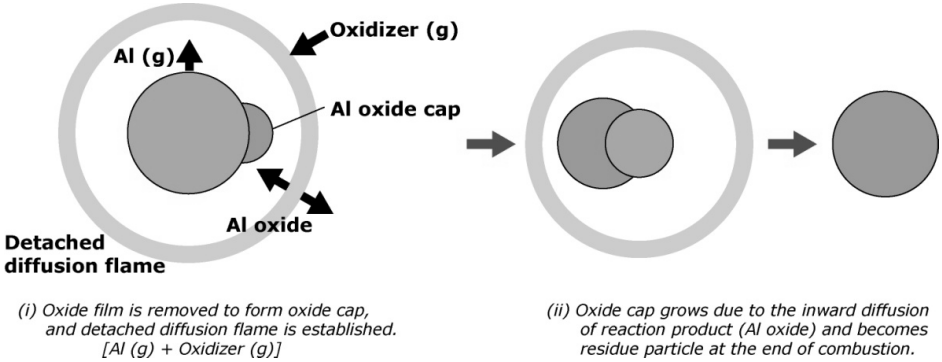

(b) Schematic for quasi-steady combustion stage with detached diffusion flame to form residue particle

Fig. 1. Schematics for ignition and quasi-steady combustion stage.

Studies on the aluminum particle combustion have largely centered on elucidating combustion characteristics of aluminum powder as an additive to enhance the specific impulse or alleviate wave instabilities of the solid propellants [7]. These earlier works were extended to more rigorous studies on the ignition and combustion of aluminum particles as a fuel of high energy density. Effects of the oxide film and initial particle size on the ignition delay were experimentally investigated. A correlation for the locus of ignition temperature in terms of particle size and oxygen content was presented [8]. A smaller particle and an oxidizer rich mixture were more favorable to the particle ignition. Razdobreev et al. [9] attempted microphotography and CO_2 laser heating method. High-resolution images evidenced that the ignition is locally initiated and propagates over the entire particle surface with a velocity which depends on the particle size. The metal particle ignition characterized by thin oxide layer and self-heating is well expressed in terms of Maragoni number [10]. Fedorov et al. [11] adopted semi-empirical oxidation laws, and proposed an ignition model which includes exothermic growth of oxide film. Theoretical and numerical models for quasi-steady aluminum particle burning are numerous. Glassman [12] reported that the metal particle combustion is analogous to that of the liquid droplet burning hence D^2-law can be applied. Law [13] suggested a combustion model which employs a general frame of the hydrocarbon droplet combustion model featured by a diffusion-controlled spherically symmetric envelope flame. Liang et al. [14] conducted two-dimensional numerical model which incorporates variable transport properties, and predicted the condensation of aluminum oxide and the oxide cap growth. Fabignon et al. [15] proposed a three-dimensional axisymmetric model based on the formulation of the energy balance at the particle surface. In their rigorous five-zone model, Babuk et al. [16] formulated the oxide cap growth by inward diffusion of the aluminum oxide. Melcher et al. [17] experimentally investigated the effect of convective gas flows on the particle combustion.

Initial oxide film causes ignition delay and it melts to form an oxide cap on the particle surface, which affects the quasi-steady combustion. The ignition of the aluminum particle begins with a heterogeneous combustion [4] and quickly transits into the quasi-steady combustion regime featured by a detached spherical diffusion flame positioned off the particle surface at two to five radii [18, 19]. Hence the formulation of the ignition and quasi-steady burning in an integrated frame is essential to a realistic modeling of the aluminum particle combustion. But, the studies on the unified modeling are very limited. Marion et al. [20] carried out an experiment for laser-induced ignition and combustion of an isolated aluminum particle suspended in an electro-dynamic levitator. Desjardin [21] proposed a simple mechanistic model which comprehends both the ignition and the quasi-steady combustion. This model includes the ignition and the QSC in a single frame, but did not appreciate all characteristics of aluminum particle

combustion.

As stated above, the phenomena and mechanism of the aluminum particle combustion have been figured out through various analytical or experimental researches and a few numerical models have been developed. But most of the previous studies centered on either ignition or quasi-steady combustion separately and the rigorous numerical studies are computationally heavy to describe every details regarding the aluminum oxide. The most recent model was simple and considered both ignition and quasi-steady combustion process, but it was ambiguous and insufficient to represent all the characteristics of Al particle combustion. Furthermore, it is required to couple with Computational Fluid Dynamics (CFD) simulation for system application, and the model should be simple and adaptable to appropriate CFD method like an Arbitrary Lagrangian-Eulerian (ALE) method as well as realistic one describing the phenomena. In the present study, therefore, a simplified analytical modeling of single aluminum particle combustion was conducted. Ignition and quasi-steady combustion (QSC) stages were formulated in conjunction with the transport equations for droplet combustion [12, 13, 22, 23]. Initial oxide film and its effect on the ignition were treated in a rigorous manner. Heat transfer from the hot ambient gas and enthalpy of heterogeneous surface reaction (HSR) were regarded as the energy sources for particle ignition. Assuming gas-phase reaction of aluminum vapor in air, conservation equations were solved for QSC parameters in conjunction with conserved scalar formulation and Shvab-Zeldovich function. To serve a limit temperature postulate, a sink term describing dissociation of reaction product near the flame zone was freshly added in the evaluation of flame temperature. Effective latent heat of vaporization [24] was modified to include the radiative heat transfer during quasi-steady burning. Thermodynamic and transport properties were expressed as a function of temperature and iterative method were resolved for accuracy and rationality. Ignition and QSC of the aluminum particle were predicted and discussed with emphasis on the effect of the aluminum oxide and variable properties.

2. Modeling of an aluminum particle combustion

Principal aim of the present study is the development of a practical and simple mechanistic model of the combustion of single aluminum particle. The model comprehends every commanding processes, but is computationally cost-effective than previous analytical models [14-16, 25].

Combustion of single aluminum particle is modeled in two stages of ignition (oxide film removal) and quasi-steady combustion. Essential processes including ignition delay, heterogeneous surface reaction, convective and radiative heat transfer, gas phase reaction (homogeneous reaction), inward and outward diffusion of reaction product, and formation of residue particle are formulated and incorporated into the model.

2.1 Initial aluminum particle

For the convenience of the model validation and comparison with other models, the aluminum particle is assumed to be a sphere of 165 μm of its initial diameter. Typically, prolonged exposure of a pure aluminum to a low (room) temperature oxidizer gas results in the formation of a thin layer of amorphous aluminum oxide (alumina) on the aluminum particle [26, 27]. Thickness of this naturally-formed oxide film might be lower at 0.5 nm or higher up to 4 nm [28, 29], but typically lies in a narrow range from 2 nm to 3 nm [30, 31]. In this narrow range, an alteration of the ignition profile due to the film thickness seems to be much less probable and thus 3 nm of the initial oxide film thickness was assumed.

2.2 Oxide film removal and ignition

The oxide film isolates pure aluminum from the oxidizer, and thus it prevents an unexpected ignition. On the other hand the oxide film gives rise to the ignition delay because melting temperature of the oxide (~2200K) is much higher than that of the aluminum. No ignition occurs until the oxide film melts and peels back (Fig. 1(a)). Similar to the ignition of a magnesium particle, the ignition may be initiated after the cracking of oxide film [32, 33], but the removal of the oxide film concurrent with the oxide melting would be more probable cause for the particle ignition [3, 34] when the particle size is a few hundreds of microns in particular.

The general frame of the ignition model is similar to the previous model [35]. During the ignition period, convective and radiative heat transfer from ambient hot gas (external heat source) increases the particle temperature. The HSR occurs at the particle surface and supplies additional energy (internal heat source). Thus, the particle temperature is determined by convective and radiative heat transfer, HSR, fusion of aluminum core.

In Eq. (1), all thermo-physical properties depend on the temperature. Since an ambient gas (air) temperature is a priori (Table 1), the evolution of particle temperature is readily obtained by solving Eq. (1) in conjunction with the infinite conductivity [36, 37] and the effective specific heat of the particle ($c_{p,p}$). The particle which consists of Al (s) and Al_2O_3 (s) is heated up and both the transferred heat from hot ambient and the enthalpy of HSR are spent to increase the temperature of aluminum core until it reaches its melting point. During the period of aluminum core melting, the particle temperature remains unchanged at its saturation point ($T_{Al,melt}$) and the mass fraction of the liquid aluminum ($\alpha \equiv m_l/(m_l+m_s)$) rises from zero to one. Here, α measures an extent of aluminum core melting and the occurrence of HSR. Once the metal core is melted away into the liquid ($\alpha = 1$), the particle temperature rises again. Rate of aluminum fusion ($\dot{m}_{Al,sl}$) is ;

$$m_p c_{p,p} \frac{dT_p}{dt} = \dot{Q}_{conv} + \dot{Q}_{rad} - \dot{Q}_{Al,melt} + \dot{Q}_{HSR} = 2\pi r_p \frac{\mu_g c_{p,g}}{\mathrm{Pr}_g}\left(T_g - T_p\right) Nu_p + \varepsilon_{Al}\sigma\left(T_g^4 - T_p^4\right) A_p - \dot{m}_{Al,sl} h_{Al,sl} - \dot{m}_{Al,HSR} h_{r,HSR} \quad (1)$$

$$\dot{m}_{Al,sl} = \begin{cases} \left(\dfrac{\dot{Q}_{conv} + \dot{Q}_{rad} + \dot{Q}_{HSR}}{h_{sl}} \right) & \text{for } 0 \le \alpha < 1,\ T_p = T_{Al,melt} \\ 0 & \text{otherwise} \end{cases} \quad (2)$$

The rate of HSR ($\dot{m}_{Al,HSR}$) is expressed in an Arrhenius-type of formulation with experimentally determined pre-exponent coefficient and activation energy [38]. Occurrence of the HSR is valid only after the initiation of the melting ($\alpha > 0$) and thus $\dot{m}_{Al,HSR}$ is zero otherwise.

$$\dot{m}_{Al,HSR} = \begin{cases} \left[A_p A_1 \exp\left(-E_a / R_u T_p \right) \right] & \text{for } \alpha > 0 \\ 0 & \text{otherwise} \end{cases} \quad (3)$$

The ignition is terminated when the particle temperature rises over the melting point of aluminum oxide. Details of the solution procedure are shown in the appendix.

2.3 Quasi-steady combustion

Immediately after the termination of the ignition stage, the oxide film is instantly peeled off and the liquid oxide coalesces into a cap on the particle surface. Molten aluminum core is readily exposed to the gaseous oxidizer and the combustion enters into QSC stage featured by a diffusion flame standing off the particle.

For simplicity, spherically symmetric particle geometry and flame sheet approximation are incorporated into the formulation of the QSC. With this tailored problem configuration, the oxide cap growth and the formation of the residue particle are expressed in terms of the mass of aluminum oxide deposited on the particle surface only. To this end, a sink term ($\dot{S}$) to include the effect of the inward diffusion of the reaction product and the oxide cap growth is newly added to the mass conservation equation. Continuous deposition of the metal oxide on the aluminum droplet is formulated with an extended conserved scalar and a modified Shvab-Zeldovich function. This simple calculation method is computationally inexpensive and thus it would be easily incorporated into ALE (Arbitrary Lagrangian-Eulerian) computation for system application.

Transports of the mass and the energy during QSC of aluminum droplet with the oxide cap are illustrated in Fig. 2(a) and 2(b), respectively. Radial binary diffusion is formulated by Fick's law for an ordinary diffusion.

$$\dot{m}''_{i,s} = Y_{i,s} \dot{m}''_{tot,s} - \rho D_m \left(\frac{dY_i}{dr} \right)_s \quad (4)$$

Under the conditions of mass conservation ($\dot{m}''_{Al,s} - \dot{S}'' = \dot{m}''_{tot,s}$) and stoichiometric reaction ($\dot{m}''_{ox} = \nu \dot{m}''_{Al}$) at the flame sheet, the mass transport equation can be converted into Eq. (5) and (6) in terms of the fuel and oxidizer, respectively, and a mass transfer number (B_{Al-Ox}) between aluminum and oxidizer can be obtained (Eq. (7)).

$$\dot{m}_{tot}'' = \left(\frac{1}{f+1} \right) \left[Y_{Al} \dot{m}_{tot}'' - \rho D_m \frac{dY_{Al}}{dr} \right] \quad (5)$$

$$\dot{m}_{tot}'' = \left(\frac{1}{f+1} \right) \left[\left(Y_{ox}/\nu \right) \dot{m}_{tot}'' - \rho D_m \frac{d\left(Y_{ox}/\nu \right)}{dr} \right] \quad (6)$$

$$B_{Al-ox} = \frac{Y_{Al,s} + Y_{ox,\infty}/\nu_{ox}}{\left(f+1 \right) - Y_{Al,s}} \quad (7)$$

Other mass transfer numbers are obtained in a similar manner and generally in a form of Eq. (8) [22, 23].

$$B_{Al-i} = \frac{Y_{i,\infty} - Y_{i,s} + \nu_i Y_{Al,s}}{\left[Y_{i,s} - \nu_i Y_{Al,s} + \nu_i \left(f+1 \right) \right]} \quad (8)$$

In Eq. (5) through (8), a non-dimensional parameter $f \left(\equiv \dot{S} / \dot{m}_{Al} \right)$ measures the fraction of the oxide mass due to the inward diffusion.

The model hires the general frame of the solution strategy in the reference [21], but newly formulated with a few modifications including a new definition of the transfer number, formulation of the radiative heat transfer by using the concept of effective latent heat of vaporization, and modeling of the oxide smoke effect.

The mass transport equations based on an assumption of the stoichiometric reaction and the definition of the transfer number in Eq. (8) are readily obtained. However, direct use of Eq. (8) for the aluminum oxide (B_{Al-mox}) yields unrealistic result because there is a discontinuity of mass transfer number at flame sheet due to the inward diffusion of aluminum oxide

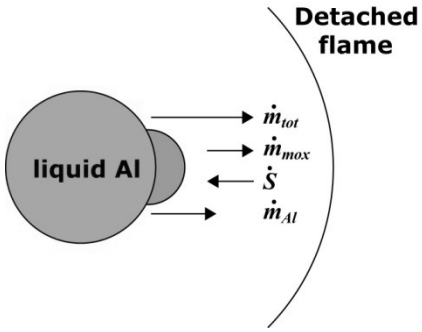

(a) Mass conservation ; inward diffusion of product ($\dot{S}$)

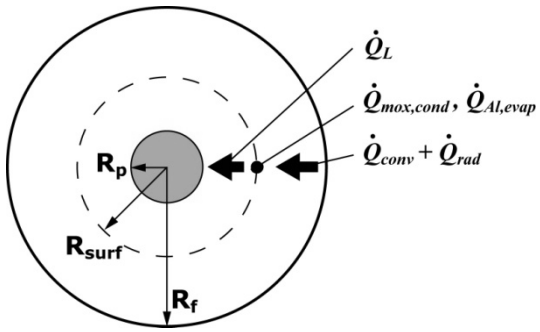

(b) Energy conservation ; heat transfer and latent heat of material

Fig. 2. Schematics for the mass and energy conservation.

($-\dot{S}'' \neq 0$) [21]. Applying stoichiometry ($\dot{m}''_{mox} = -(\nu+1)\dot{m}''_{Al}$) at the flame sheet means that gaseous reaction products diffuse inward without any outward diffusion, where all the products subsequently condense into oxide residue on the particle surface. This physically incorrect problem setup leads to an occurrence of negative oxide fraction ($f < 0$). Therefore, in the present study, the transfer number (B_{Al-mox}) is obtained from the conservation equations for total mass and the diffusion equation of oxide (i=metal oxide in Eq. (4)) instead of the stoichiometry.

$$\dot{m}_{tot}'' = \left(-\frac{1}{f}\right)\left[Y_{mox}\dot{m}_{tot}'' - \rho D_m \frac{dY_{mox}}{dr}\right] \tag{9}$$

$$B_{Al-mox} = \frac{-Y_{Al,s} - Y_{mox,s}\left(1+\frac{1}{f}\right)}{Y_{Al,s} + \left(1+\frac{1}{f}\right)Y_{mox,s} - (f+1)} \tag{10}$$

In addition, energy conservation equation is modified in order to include the radiative heat transfer. On the occasion of the particle ignition, the particle temperature is readily obtained by making use of Eq. (1) because the ambient gas temperature (T_g) is an initial condition which is known and unchanged during the ignition stage. Moreover, the radiative heat transfer is weaker than the thermal convection and HSR in ignition stage. However, the ambient gas temperature ($T_{g,r}$) is an essential state parameter in QSC and much higher than initial gas temperature (T_g). In addition, temperature increases rapidly from the particle surface to the flame front and the radiative heat transfer becomes important with the presence of high-temperature flame. Conservation of energy across the flame boundary is illustrated in Fig. 2(b). Sensible heat due to the convective and radiative heat transfer from the flame is spent for the evaporation of the aluminum, condensing aluminum oxide adds the heat and the net heat ($\dot{Q}_L$) penetrates into the particle surface. It is assumed that phase change of materials (aluminum and oxide) occur at arbitrary radial location near the particle surface. Similar to the mass transfer number, energy transfer number is formulated in terms of a conserved scalar and a modified Shvab-Zeldovich function [22].

$$B_{Al-T} = \frac{c_{p,g}\left(T_\infty - T_p\right) + H_r Y_{Al,s}}{Lh_{eff} + H_r\left(f + 1 - Y_{Al,s}\right)} \tag{11}$$

Concept of effective latent heat of vaporization (Lh_{eff}) in Eq. (11) is adopted from the literature [24], but it is modified as shown in Eq. (12) for the calculation of varying ambient temperature ($T_{g,r}$) with high-temperature flame.

$$Lh_{eff} = \frac{\dot{Q}_{conv} + \dot{Q}_{rad}}{\dot{m}_{tot}} = \frac{\dot{Q}_L - \dot{Q}_{mox,cond} + \dot{Q}_{Al,evap}}{\dot{m}_{tot}} \tag{12}$$

The effective latent heat of vaporization in Ref. [24] was defined for the formulation of the liquid droplet vaporization. The definition includes the effect of the radiative heat transfer but appropriates only to the occasion of constant-temperature atmosphere. In the present particle combustion, however, the ambient gas temperature changes due to the presence of the exothermic reaction between aluminum and the oxidizer. Then the energy conservation equation becomes a quartic function of the temperature (Eq. (13)) and is solved by iterative (Newton-Raphson) method. On this occasion, the ambient gas temperature ($T_{g,r}$) can be obtained from Eq. (11) and (13) in conjunction with the newly defined effective latent heat of vaporization in Eq. (12) and other unknown variables (Lh_{eff} , Q_L) is also obtained without additional equations or assumptions. In all equations, transport properties of the mixture gas (nitrogen gas, aluminum and alumina vapor) are functions of the temperature.

Aforementioned oxide smoke effect due to the oxide condensation and its dissociation near the outer reaction zone is also considered to evaluate flame temperature. Based on the general frame of the solution strategy in the reference [23], the limit temperature postulate is expressed by a sink term (h_{disso}) in Eq. (14).

$$\dot{Q}_L = \dot{Q}_{conv} + \dot{Q}_{rad} + \dot{Q}_{mox,cond} - \dot{Q}_{Al,evap} = \left[2\pi r_p \frac{\mu_g c_{p,g}}{\mathrm{Pr}_g}\left(T_{g,r} - T_p\right)\cdot Nu_p\right] + \left[A_p \cdot \varepsilon\sigma\left(T_{g,r}^4 - T_p^4\right)\right] + \left(\dot{S}\cdot h_{mox,gl}\right) - \left(\dot{m}_{Al} h_{Al,\mathrm{lg}}\right) \tag{13}$$

$$T_f = \exp\left(-\frac{Sc\cdot\dot{m}_{tot}}{4\pi r_f \mu_g}\right)\left[\left(T_\infty - T_p\right) + \frac{Lh_{eff} + H_r(f+1) - h_{disso}\left(\dot{m}_{mox,out}/\dot{m}_{tot}\right)}{c_{pT}}\right] - \left[\frac{Lh_{eff} + H_r(f+1) - h_{disso}\left(\dot{m}_{mox,out}/\dot{m}_{tot}\right)}{c_{p,g}}\right] + T_p \tag{14}$$

The oxide mass ($\dot{m}_{mox,out}$) due to its outward diffusion is simply the total mass of reaction product subtracted by the oxide mass due to its inward diffusion (Fig. 3). Only a global reaction between the gaseous aluminum and the oxygen in an inert nitrogen gas is solved for the enthalpy of reaction (H_r) and the Brzustowski's assumption [1] is adopted to find the dissociation energy of Al_2O_3 [39].

$$2Al(g) + \tfrac{3}{2}O_2(g) \xrightarrow{\Delta h=-2280\mathrm{kJ/mol}} Al_2O_3(l) \tag{15}$$

$$Al_2O_3(l) \xrightarrow{\Delta h=2017.2\mathrm{kJ/mol}} AlO(g) + Al(g) + O_2(g) \tag{16}$$

Finally, iterative method to find the combustion parameters is improved. In the previous study [21], mass fraction of aluminum vapor near the particle surface ($Y_{Al,s}$) was a single iteration variable and it was uncertain whether the oxide mass fraction (f) would be physically correct inside of the iteration loop. To this end, another iteration loop to calculate the oxide mass fraction is added, and this excludes the unrealistic assumption such as zero mass fraction of the aluminum oxide

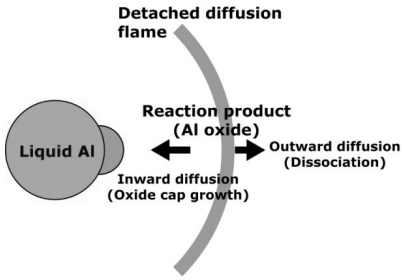

Fig. 3. Schematic of the reaction product effects; oxide cap growth by inward diffusion and limiting flame temperature by outward diffusion.

near the particle surface (=assumption of very fast oxide deposition [13], $Y_{mox,s}=0$). Previously, an assumption of $Y_{mox,s}=0$ was a prerequisite to close the formulation because the oxide fraction (f) was a function of mass fraction of various materials (aluminum, oxide, oxidizer, etc) at the particle surface. In the present model, however, only the relations among the particle temperature, the aluminum vapor pressure and $Y_{Al,s}$ are required because the f is a variable which is iteratively obtained. Solution procedures for the quasi-state combustion are detailed in the appendix.

2.4 Transport and thermodynamic properties

It is easily expected that particle temperature which evolves in a wide range from 300K to 2200K causes substantial changes in the material properties hence every thermophysical property is expressed as a function of temperature for the calculation accuracy. Time-dependent conservation equations for mass and energy are solved for particle transients with a full account of variable properties. Due to the lack of data, the latent heat, the densities of aluminum and alumina were assumed to be constant. Unitary Lewis number assumption is used for simplicity. National Institute of Standard and Technology (NIST) data base and Chapman-Enskog kinetic theory [40] are used in order to find the specific heat and other transport properties, respectively, in conjunction with the data of the liquid alumina [41]. Mixing rules are typical:

$$\rho_{mix}=\left(\frac{\overline{Y}_{vap}}{\rho_{vap}}+\frac{1-\overline{Y}_{vap}}{\rho_{gas}}\right)^{-1} \tag{17}$$

$$c_{p,mix}=c_{p,vap}\overline{Y}_{vap}+c_{p,gas}\left(1-\overline{Y}_{vap}\right) \tag{18}$$

$$\mu_{mix}=\sum_{i=1}^{n}\frac{x_i\mu_i}{\sum_{j=1}^{n}x_j\Phi_{ij}} \tag{19}$$

$$k_{mix}=\sum_{i=1}^{n}\frac{x_i k_i}{\sum_{j=1}^{n}x_j\Phi_{ij}} \tag{20}$$

$$\Phi_{ij}=\frac{\left[1+\left(\frac{\mu_i}{\mu_j}\right)^{1/2}\left(\frac{M_j}{M_i}\right)^{1/4}\right]^2}{\sqrt{8}\left[1+\left(\frac{M_i}{M_j}\right)\right]^{1/2}}$$

(x_j : mole-fraction, M_j : molar mass)

Table 1. Test matrix and configuration.

Conditions	Values
Initial particle diameter	165
Initial particle temperature	300 K
Ambient gas	Air (N_2+O_2 gas)
Ambient air flow	quiescent air / free falling paritcle
Ambient pressure	1 atm
Ambient temperature (5 case)	1000, 1500, 2000, 2500, 3000 K

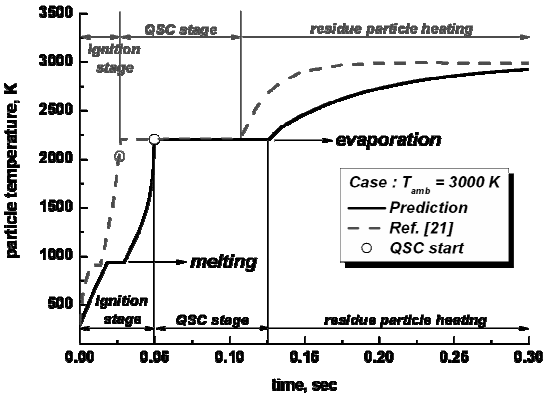

Fig. 4. Evolution of the particle temperature (T_{amb} = 3000K).

3. Results and discussion

Ignition and burning of an aluminum particle free falling in an oxidizer gas are analytically investigated. The aluminum particle initially covered with thin oxide film is suddenly introduced into an ambient air of the temperature in the range of 1000K to 3000K. Initial diameter and temperature of the particle are 165μm and 300K, respectively. Essential geometrical and thermodynamic conditions are summarized in Table 1. This problem configuration repeats previous modeling condition aiming at the convenience of model validation and comparison of the prediction accuracy. Evolutions of particle temperature and diameter, fractions of molten aluminum and aluminum oxide are calculated. Burning rate, combustion time, flame radius and temperature are also predicted and compared with the measurements.

In Fig. 4, plots of evolving temperature of an aluminum particle burning in air of 3000K are shown and compared. The particle heats up until its temperature reaches at the melting point of aluminum and the temperature is unchanged during the period of aluminum core melting (t=0.018~0.029 sec) because all the transferred heat is spent for supplying latent heat of fusion. Since the liquid (or vapor) aluminum core is isolated from the oxidizer by passivative solid oxide film, no reaction between the gaseous aluminum and the oxidizer occurs. In this period, however, partial exposure of the liquid aluminum to the oxidizer gives rise to HSR ($\alpha>0$) which fills the role of the primary heat source for the ignition. Since

Table 2. Comparison of ignition delay, QSC duration, burning rate and particle temperature in QSC stage.

T_{amb} (K)	Previous results [21]				Predicted results			
	$t_{ignition}$ (sec)	t_{QSC} (sec)	Averaged burn rate $\left(\times 10^{-7}\, m^2/\sec\right)$	$T_{p,QSC}$ (K)	$t_{ignition}$ (sec)	t_{QSC} (sec)	Averaged burn rate $\left(\times 10^{-7}\, m^2/\sec\right)$	$T_{p,QSC}$ (K)
1000	not ignited	-	-	-	0.9255	0.082	-3.1800	2200.7
1500	0.1114	0.1226	-2.2178	2194.3	0.1922	0.082	-3.2384	2202.2
2000	0.0570	0.1038	-2.5642	2205.4	0.1051	0.080	-3.3254	2203.5
2500	-	-	-	-	0.0692	0.078	-3.4139	2202.2
3000	0.0256	0.0811	-3.2959	2216.8	0.0497	0.076	-3.5058	2202.4

the activation of HSR strongly depends on the particle temperature (Eq. (3)), short ignition delay is expected at high ambient temperature. An exponential increment of the particle temperature as the time elapses to 0.05 sec manifests that the HSR is progressively activated and provides heats for the ignition. As the particle temperature rises over 2200K, the oxide film is removed and the particle is ignited. Then the quasi-steady combustion is initiated and the process transits from the ignition into diffusion controlled combustion regime. The QSC of an aluminum particle resembles to typical droplet combustion while the droplet temperature is unchanged due to the evaporation of aluminum droplet (t=0.049~0.126 sec). Immediately after the termination of the QSC, the residue alumina particle is heated up to the ambient gas temperature.

In Table 2, ignition delay, duration of QSC and burning rate at different ambient gas temperature are shown and compared with previous results [21]. Both models predicted the particle temperature to be near 2200K during QSC period regardless of the initial ambient temperature because all the heat is spent for evaporating the aluminum droplet. The ignition delay strongly depends on the ambient gas temperature hence is shortened with increasing in the ambient gas temperature because activation of HSR is retarded at lower ambient gas temperature. It is noted that an occurrence of the ignition at very low ambient gas temperature of 1000K is predicted by the present model but not in the previous study. The ambient gas temperature of 1000K is not high enough to activate HSR but still higher than the melting temperature of the aluminum core and thus fulfills the condition for an occurrence of HSR ($\alpha > 0$). In this case, the HSR is a sole heat source for ignition and the ambient gas becomes a heat sink once the particle temperature rises over 1000K. In the present calculation, the heat generated by HSR is a little greater than heat lost by convection and radiation, hence the particle is ignited though it takes long time for heating the particle to activate the HSR. Once the envelope flame is built, the evaporation (burning) rate of the liquid aluminum depends on the flame temperature rather than the initial ambient gas temperature and thus remains almost unchanged during the QSC. Duration of the QSC is also almost unchanged regardless of initial ambient gas temperature due to the steadiness of burning rate.

At all ambient gas temperatures, the present model predicts longer ignition delay roughly twofold of the previous result (Table 2). For model validation, theoretical equation for the ignition delay of the aluminum particle is adopted. In their study, Friedman et al. solved a heat conduction equation to find an ignition delay time (Eq. (21)) and validated with the measurements [34].

$$t_{ig} = \frac{\rho_{Al} r_p^2}{3k_g}\left[c_{p,g} \ln\left(\frac{T_\infty - T_{p0}}{T_\infty - T_{ig}} \right) + \frac{h_{Al,sl}}{T_\infty - T_{Al,melt}} \right] \tag{21}$$

In Eq. (21), $k_g = \left(2.4\times 10^{-5}\right)\times\left(T_\infty / T_{p0}\right)$ kJ/m-sec-K is thermal conductivity of the gas, T_{ig} is ignition temperature, and $c_{p,g}$ is average heat capacity of the gas in the temperature range from T_{p0} to T_{ig}. The application of Eq. (21) is limited since the ambient gas temperature (T_∞) must be higher than the ignition temperature (T_{ig}). It was stated in the Ref. [34] that the ignition delay (t_{ig}) was sensitive to the ignition temperature (T_{ig}) and must be selected carefully. T_∞ and T_{ig} were 2510K and 2300K, respectively. Boiko et al. [42] carried out an experiment for self-ignition of aluminum powder heated by the shock wave (T_{ig}=1800K.), and concluded that the ignition delay time predicted by Eq. (21) agrees well with the experiment. In Fig. 5, solid line is the plot of Eq. (21) in the case of T_{ig}=2200K and solid square and triangle are predicted ignition delay times of the present model and the reference [21], respectively. It is obvious that predictions considerably deviate from the theoretical plot particularly when the ambient temperature is less than 2500K, but gradually comes to close as the temperature rises. Comparing with the data in the reference [21], the ignition delay time predicted by the present model (solid square) is closer to the plot of Eq. (21) and converges to the theoretical plot as the temperature increases. It has been reported that the characteristics of aluminum ignition is rarely influenced by the initial oxide film thickness [43]. Besides, both models include the description on the initial oxide film hence the presence of the oxide film is not a primary cause for such large difference in the prediction. More probable reason would be the use of constant transport properties and dimensionless numbers such as Prandtl number and Schmidt number fixed at 0.613 without any rationale [21]. From its introduction into the hot ambient gas to the formation of the residue particle, the aluminum particle experiences rapid increase in the temperature from 300K to 2200K concurrent with large changes in the thermo-physical properties. For ex-

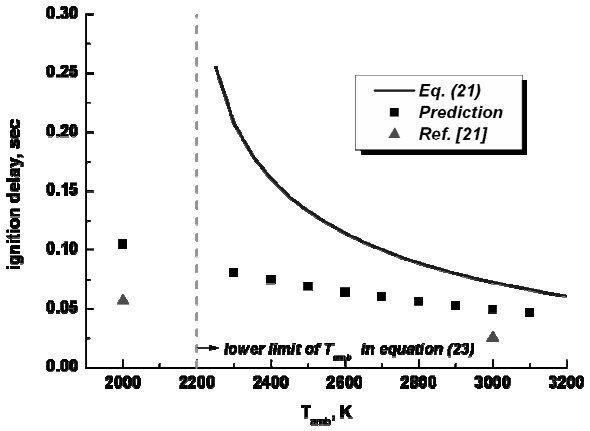

Fig. 5. Comparison of ignition delay time.

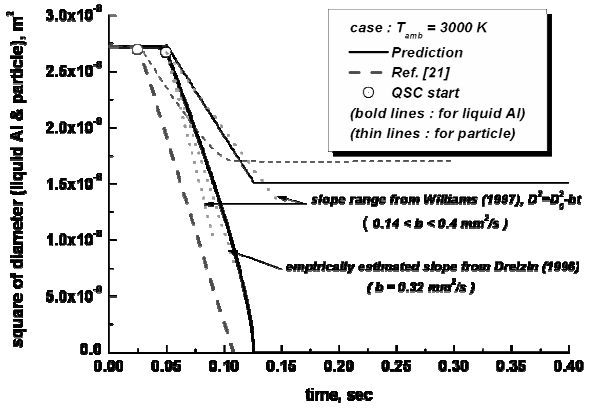

Fig. 6. Evolution of particle diameter (T_{amb} = 3000K).

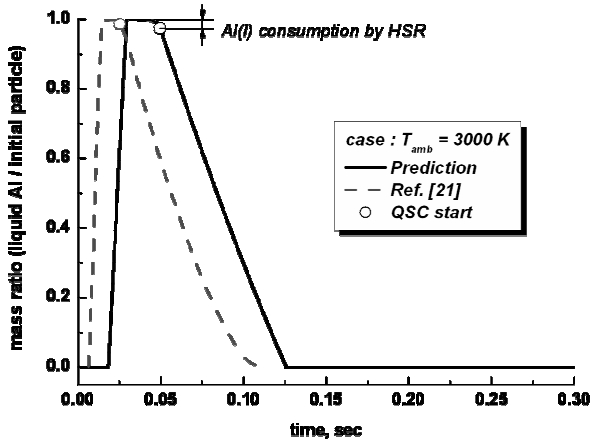

(a) Ratio of the liquid aluminum to initial particle mass

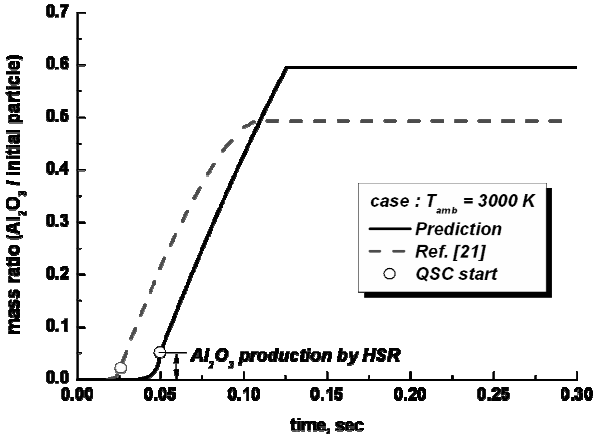

(b) Ratio of the aluminum oxide to initial particle mass

Fig. 7. Evolution of the mass ratio of Al (l) and Al_2O_3 to the initial particle (T_{amb} = 3000K).

ample, the specific heat of particle varies from 0.89 to 1.35 kJ/kg-K in this temperature range and most of other transport properties are also strong functions of the temperature [44].

History of the particle diameter is portrayed in Fig. 6. Even with the presence of oxide film, the particle (aluminum +oxide) diameter is almost same with the diameter of pure aluminum droplet because the oxide film is very thin (δ =3 nm). Diameter of aluminum core is slightly decreased immediately before the entrance into QSC stage because the HSR consumes part of the liquid aluminum during ignition period but the particle diameter is slightly increased due to the product of HSR. After the commencement of QSC, the particle surface regresses because of the evaporation of the liquid aluminum. But the evaporation rate (slope of the D^2-curve) of liquid aluminum droplet (bold line) is distinguished from the decreasing rate of the particle surface area (thin line) due to the inward diffusion and deposition of the combustion product to form a residue particle. At 3000K, the burning rate of the liquid aluminum droplet lies within the range of experimental result of Williams [19] and agrees well with the experiment by Dreizin [45]. In addition, burning rates at various ambient gas temperatures (Table 2) lie within the range of the previous experimental result. The oxide cap grows due to the deposition of reaction product on the particle surface and remains as a residue particle after the completion of burning. The size of the residue particle is in the range from 1/2 to 2/3 of the initial particle diameter [46], and both models correctly predict the residue particle size in this range.

Fig. 7(a) and (b) show histories of the mass ratio of liquid aluminum and aluminum oxide to the initial particle at the ambient gas temperature of 3000K, respectively. At the beginning of ignition stage, no HSR occurs and the particle is heated by the convective and radiative heat transfers only. As the temperature rises over the melting point of aluminum, the aluminum core melts and exothermic HSR occurs and then the particle temperature increases exponentially (Fig. 4). Concurrent with rising temperature, the HSR is more activated and it consumes small amount of the liquid aluminum (Fig. 7(a)) hence fraction of the aluminum oxide increases during the ignition stage (Fig. 7(b)). Mass ratio of the liquid aluminum is always less than unity because the mass fraction of the oxide is not initially zero and the liquid aluminum is consumed by the HSR as well as the quasi-steady combustion.

Similarly, the mass ratio of the aluminum oxide is always greater than zero because of the presence of the initial oxide

Table 3. Dependence of mass ratio of Al and Al_2O_3 on the ambient gas temperature in HSR.
(Mass ratio between Al (or Al_2O_3) and initial particle)

	Previous results [21]		Predicted results	
	Al	Al_2O_3	Al	Al_2O_3
1000	-	-	-0.0684	+0.130
1500	0	+0.027	-0.0413	+0.078
2000	0	+0.020	-0.0345	+0.065
2500	-	-	-0.0302	+0.057
3000	-0.0075	+0.014	-0.0269	+0.051

Table 4. Predicted flame radius and temperature at various ambient temperature.

T_{amb} (K)	r_f / r_{p0}	T_f (K)
1000	4.60~4.66	3196.8
1500	4.83~4.89	3447.8
2000	5.06~5.09	3711.3
2500	5.28~5.30	3952.7
3000	5.51~5.52	4224.1
Reference	2~5	3500~4200

Table 5. QSC duration at various ambient gas temperature.

T_{amb} (K)	t_c (sec) [21] (Previous)	t_c (sec) (Prediction)	t_c (sec) [15] (Correlation)
1000	-	0.082 (-8.65%)	0.089
1500	0.1226	0.082 (-5.41%)	0.087
2000	0.1038	0.080 (-4.58%)	0.084
2500	-	0.078 (-4.15%)	0.081
3000	0.0811	0.076 (-3.64%)	0.079

film and continuous inward diffusion of reaction product. Dependence of HSR on the ambient gas temperature is summarized in Table 3. As expected, the ignition is further delayed at lower ambient gas temperatures and the increase in the consumption (or production) of aluminum (or oxide) is observed because of extended duration of HSR at lower temperatures. It is inferred that overestimation of the HSR extent comparing with the previous result, namely more amount of Al_2O_3 production, is mainly due to the prediction of longer ignition delay time.

Flame radius and flame temperature are predicted in terms of ambient gas temperature and the results are shown in Table 4. As stated, a detached flame is positioned off the particle surface at two to five radii and it is slightly overestimated by 10 percent in the case of 3000K. The flame temperatures which have been reported to lie within the range of 3500~4200K [13-16, 18, 25] are well predicted. The flame temperature is underestimated by 10 percent in the case of 1000K.

Duration of QSC was calculated using the correlation suggested by Fabignon [15] and compared with the prediction at various ambient temperatures in Table 5. Agreement is satisfactory and prediction errors are less than 10%. According to the Belyaev et al. [47], the QSC duration less depends on the ambient gas temperature because the heat of aluminum oxidation reaction is high and it commands the combustion. In Table 5, the predicted burning durations are almost unchanged at different ambient gas temperatures.

4. Conclusion

A simplified analytical modeling of single aluminum particle combustion was conducted. Based on the previous method [21], thermal radiation and oxide smoke effect were freshly incorporated into the transport equations in conjunction with new definitions of transfer number and effective latent heat of vaporization. Ignition and quasi-steady combustion (QSC) stages were formulated and predicted with emphasis placed on the effect of the aluminum oxide and variable properties.

Model validation regarding the ignition delay was made and the agreement was satisfactory particularly at high ambient gas temperatures. Evaporation rate, residue particle size, flame temperature, QSC duration, and stand-off distance of the envelop flame were also compared with the measurements. The predictions yielded good agreement within approximately 10 percent error and enhancement of the prediction accuracy remained as a future task. It might be meaningful that the present modeling considered whole combustion process and described almost all of the characteristics for aluminum particle combustion related with aluminum oxide with low computational load in simplicity. This simplified model will be more tailored to be incorporated into an ALE simulation of the industrial aluminum particle laden Al-air and Al-water flame.

Acknowledgements

This work was supported by Defense Acquisition Program Administration and Agency for Defense Development under the contract UD070027AD.

Nomenclature

δ	:	Oxide film thickness
ε	:	Emittance
μ	:	Viscosity
ν	:	Stoichiometric ratio
ρ	:	Density
σ	:	Stefan-Boltzmann constant
A	:	Surface area
A_1	:	Pre-exponential coefficient
c_p	:	Specific heat
D_m	:	Mass diffusivity
d	:	Diameter
E_a	:	Activation energy
f	:	Mass ratio between inward diffusion of oxide and total mass transfer
H_r	:	Enthalpy of reaction (gas phase reaction)

h : Latent heat of phase change
h_{diss} : Enthalpy of dissociation
$h_{r,HSR}$: Enthalpy of reaction for HSR
k : Thermal conductivity
m : Mass
$\dot{m}$: Mass rate
Lh_{eff} : Effective latent heat of vaporization
$p_{Al,vap}$: Aluminum vapor pressure
$\dot{Q}$: Heat transfer
R_u : Universal gas constant
r : Radius
$\dot{S}$: Oxide inward diffusion rate $\left(=-\dot{m}_{mox}\right)$
T : Temperature
t : Time
Y : Mass fraction
Pr : Prandtl number
Sc : Schmidt number
Nu : Nusselt number
(s) : Solid phase
(l) : Liquid phase
(g) : Gas phase

Superscript

" : Flux

Subscript

amb : Ambient condition
p : Particle
$drop$: Droplet
i : Species
Al : Aluminum
ox : Oxidizer
mox : Aluminum oxide
mix : Mixture
tot : Total
c : Combustion
$conv$: Convection
rad : Radiation
HSR : Heterogeneous surface reaction
g : Gas or gas mixture
sl : Phase change from solid to liquid
gl : Phase change from gas to liquid
lg : Phase change from liquid to gas
s : Surface
f : Flame
∞ : Far field / ambient
$melt$: Melting
$cond$: Condensation
$evap$: Evaporation
L : Penetration
$p0$: Initial particle
0 : Initial state

References

[1] T. A. Brzustowski and I. Glassman, Vapor-phase diffusion flames in the combustion of magnesium and aluminum: I. Analytical developments, *Heterogeneous Combustion Conference*, Palm beach, Florida, (1963) 1-14.

[2] T. A. Brzustowski and I. Glassman, vapor-phase diffusion flames in the combustion of magnesium and aluminum: II. Experimental observations in oxygen atmospheres, *Heterogeneous Combustion Conference*, Palm beach, Florida, (1963) 1-14.

[3] M. A. Trunov, M. Schoenitz and E. L. Dreizin, Effect of polymorphic phase transformations in alumina layer on ignition of aluminium particles, *Combustion Theory and Modelling*, 10 (4) (2006) 603-623.

[4] M. A. Trunov, M. Schoenitz, X. Zhu and E. L. Dreizin, Effect of polymorphic phase transformations in Al2O3 film on oxidation kinetics of aluminum powders, *Combustion and Flame*, 140 (4) (2005) 310-318.

[5] E. L. Dreizin, Experimental study of aluminum particle flame evolution in normal and micro-gravity, *Combustion and Flame*, 116 (3) (1998) 323-333.

[6] E. L. Dreizin, Phase changes in metal combustion, *Progress in Energy and Combustion Science*, 26 (1) (2000) 57-78.

[7] J. C. Melcher, R. L. Burton and H. Krier, Combustion of Aluminum Particles in Solid-Rocket Motor Flows, *Progress in astronautics and aeronautics*, 185 (2000) 723-748.

[8] M. A. Gurevich, K. I. Lapkina and E. S. Ozerov, Ignition limits of aluminum particles, *Combustion, Explosion, and Shock Waves*, 6 (2) (1972) 154-157.

[9] A. A. Razdobreev, A. I. Skorik and Y. V. Frolov, Ignition and combustion mechanism in aluminum particles, *Combustion, Explosion, and Shock Waves*, 12 (2) (1977) 177-182.

[10] D. Meinkohn and G. A. C. Dlr, Oxide Layer Effects in Metal Particle Combustion, *Proceedings of the 5th International Microgravity Combustion Workshop*, Cleveland, Ohio, (1999) 219-222.

[11] A. V. Fedorov and Y. V. Kharlamova, Ignition of an Aluminum Particle, *Combustion, Explosion and Shock Waves*, 39 (5) (2003) 544-547.

[12] I. Glassman, Metal combustion processes, *AFOSR-TN-59-1093, Aeornautical Engineering Laboratory*, (1959).

[13] C. K. Law, A simplified theoretical model for the vapor-phase acombustion of metal particles, *Combustion Science and Technology*, 7 (5) (1973) 197-212.

[14] Y. Liang and M. W. Beckstead, Numerical simulation of unsteady, single aluminum particle combustion in air, *34th AIAA/ASME/SAE/ASEE Joint Propulsion Conference & Exhibit*, Cleveland, OH, (1998) 1-10.

[15] Y. Fabignon, O. Orlandi, J. F. Trubert, D. Lambert and J. Dupays, Combustion of Aluminum Particles in Solid Rocket Motors, *39th AIAA/ASME/SAE/ASEE Joint Propulsion Conference and Exhibit*, Huntsville, Alabama, (2003) 1-10.

[16] V. A. Babuk and V. A. Vasilyev, Model of aluminum agglomerate evolution in combustion products of solid rocket

propellant, *Journal of Propulsion and Power*, 18 (4) (2002) 814-823.

[17] J. C. Melcher, H. Krier and R. L. Burton, Burning aluminum particles inside a laboratory-scale solid rocket motor, *Journal of Propulsion and Power*, 18 (3) (2002) 631-640.

[18] P. Bucher, R. A. Yetter, F. L. Dryer, T. P. Parr, D. M. Hanson-Parr and E. P. Vicenzi, Flame structure measurement of single, isolated aluminum particles burning in air, *Symposium (International) on Combustion*, 2 (1996) 1899-1908.

[19] F. A. Williams, *Some Aspects of Metal Particle Combustion*, Taylor & Francis, (1997).

[20] M. Marion, C. Chauveau and I. Gokalp, Studies on the ignition and burning of levitated aluminum particles, *Combustion Science and Technology*, 115 (4-6) (1996) 369-390.

[21] P. E. DesJardin, J. D. Felske and M. D. Carrara, Mechanistic model for aluminum particle ignition and combustion in air, *Journal of Propulsion and Power*, 21 (3) (2005) 478-485.

[22] I. Glassman, *Combustion, 2nd edition*, Orlando, FL (United States), Academic Press, Inc., United States, (1987).

[23] K. K. Kuo, *Principles of combustion*, Elsevier Science Pub. Co. Inc.,New York, NY, United States, (1986).

[24] W. A. Sirignano, *Fluid Dynamics and Transport of Droplets and Sprays*, Cambridge University Press, Cambridge, UK, (1999).

[25] J. F. Widener, Y. Liang and M. W. Beckstead, Aluminum combustion modeling in solid propellant environments, *35th AIAA/ASME/SAE/ASEE Joint Propulsion Conference and Exhibit*, Los Angeles, California, (1999) 1-16.

[26] L. P. H. Jeurgens, W. G. Sloof, F. D. Tichelaar and E. J. Mittemeijer, Thermodynamic stability of amorphous oxide films on metals: Application to aluminum oxide films on aluminum substrates, *Physical Review B - Condensed Matter and Materials Physics*, 62 (7) (2000) 4707-4719.

[27] L. P. H. Jeurgens, W. G. Sloof, F. D. Tichelaar and E. J. Mittemeijer, Structure and morphology of aluminium-oxide films formed by thermal oxidation of aluminium, *Thin Solid Films*, 418 (2) (2002) 89-101.

[28] L. P. H. Jeurgens, W. G. Sloof, F. D. Tichelaar and E. J. Mittemeijer, Growth kinetics and mechanisms of aluminum-oxide films formed by thermal oxidation of aluminum, *Journal of Applied Physics*, 92 (3) (2002) 1649.

[29] J. Sanchez-Lopez, A. Gonzalez-Elipe and A. Fernandez, Passivation of nanocrystalline Al prepared by the gas phase condensation method: An x-ray photoelectron spectroscopy study, *Journal of Materials Research*, 13 (3) (1998) 703-710.

[30] P. E. Doherty and R. S. Davis, Direct observation of the oxidation of aluminum single-crystal surfaces, *Journal of Applied Physics*, 34 (3) (1963) 619-628.

[31] K. Thomas and M. W. Roberts, Direct observation in the electron microscope of oxide layers on aluminum, *Journal of Applied Physics*, 32 (1) (1961) 70-75.

[32] V. A. Ermakov, A. A. Razdobreev, A. I. Skorik, V. V. Pozdeev and S. S. Smolyakov, Temperature of aluminum particles at the time of ignition and combustion, *Combustion, Explosion, and Shock Waves*, 18 (2) (1982) 256-257.

[33] Y. V. Frolov, P. F. Pokhil and V. S. Logachev, Ignition and combustion of powdered aluminum in high-temperature gaseous media and in a composition of heterogeneous condensed systems, *Combustion, Explosion, and Shock Waves*, 8 (2) (1974) 168-187.

[34] R. Friedman and A. Macek, Ignition and combustion of aluminium particles in hot ambient gases, *Combustion and Flame*, 6 (1962) 9-19.

[35] P. George and P. E. DesJardin, Effects of heterogeneous surface reactions on the ignition of aluminum particles, *42nd AIAA Aerospace Sciences Meeting and Exhibit*, Reno, Nevada, (2004) 9018-9029.

[36] B. Abramzon and W. A. Sirignano, Droplet vaporization model for spray combustion calculations, *International Journal of Heat and Mass Transfer*, 32 (9) (1989) 1605-1618.

[37] S. K. Aggarwal, A. Y. Tong and W. A. Sirigano, Comparison of vaporization models in spray calculations, *AIAA journal*, 22 (10) (1984) 1448-1457.

[38] T. Roberts, Ignition and combustion of aluminum/magnesium alloy particles in O 2 at high pressures, *Combustion and Flame*, 92 (1) (1993) 125-143.

[39] D. Tatum and K. K. Kuo, Physicochemical considerations in modeling ignition & combustion of highly non-spherical nano-sized aluminum particles, *39th AIAA/ASME/SAE/ASEE Joint Propulsion Conference and Exhibit*, Huntsville, Alabama, (2003) 1-11.

[40] R. A. Svehla, Estimated Viscosities and Thermal Conductivities of Gases at High Temperature, *TR-132, NASA*, (1962).

[41] P. F. Paradis and T. Ishikawa, Surface Tension and Viscosity Measurements of Liquid and Undercooled Alumina by Containerless Techniques, *Japanese Journal of Applied Physics*, 44 (7A) (2005) 5082-5085.

[42] V. M. Boiko and S. V. Poplavski, Self-ignition and ignition of aluminum powders in shock waves, *Shock Waves*, 11 (4) (2002) 289-295.

[43] A. G. Merzhanov, Y. M. Grigorjev and Y. A. Gal'chenko, Aluminium ignition, *Combustion and Flame*, 29 (C) (1977) 1-14.

[44] F. Incropera and D. DeWitt, *Introduction to heat transfer*, John Wiley & Sons New York, (1996).

[45] E. L. Dreizin, Experimental study of stages in aluminum particle combustion in air, *Combustion and Flame*, 105 (4) (1996) 541-556.

[46] E. C. Ruttenberg, Burning Characteristics of Individual Aluminum/Aluminum Oxide particle *Aeronautics and Astronautics Dept.*, Naval Postgraduate School, Monterey, California, (1996) 1-48.

[47] A. F. Belyaev, Y. V. Frolov and A. I. Korotkov, Combustion and ignition of particles of finely dispersed aluminum, *Combustion, Explosion, and Shock Waves*, 4 (3) (1971) 182-185.

Appendices

(Procedure for ignition stage)

(1) Calculate liquid aluminum mass ($m_{Al,(l)}$), mass ratio (α) and solid aluminum mass ($m_{Al,(s)}$).

$$\frac{dm_{Al,(l)}}{dt} = \dot{m}_{sl} - \dot{m}_{ls}$$

$$\frac{d\alpha}{dt} = \frac{1}{m_{Al,(l)} + m_{Al,(s)}}\left[\dot{m}_{sl} - (1-\alpha)\dot{m}_{ls}\right]$$

$$\frac{dm_{Al,(s)}}{dt} = -\dot{m}_{sl}$$

(2) Calculate total particle mass (m_p) and metal oxide mass (m_{mox}).

$$\frac{dm_p}{dt} = \nu_{ox}\dot{m}_{ls} \quad , \quad m_p = m_{Al,(s)} + m_{Al,(l)} + m_{mox}$$

(3) Calculate Particle velocity (u_p) and Non-dimensional number (Re, Pr, Nu).

$$\mathrm{Re}_p = \frac{\rho_g u_p d_p}{\mu_g} \quad , \quad \mathrm{Pr}_g = \frac{\mu_g c_{p,g}}{k_g}$$

$$Nu_p = \begin{cases} 1 + \left[1 + \mathrm{Re}_p \mathrm{Pr}_g\right]^{1/3} & (\mathrm{Re} \le 1) \\ 1 + \left(\mathrm{Re}^{0.077}\right) \cdot \left[1 + \mathrm{Re}_p \mathrm{Pr}_g\right]^{1/3} & (\mathrm{Re} \le 400) \\ 2 + 0.552\,\mathrm{Re}_p^{1/2}\,\mathrm{Pr}_g^{1/3} & (\mathrm{Re} > 400) \end{cases}$$

$$C_D = \begin{cases} \dfrac{24}{\mathrm{Re}}\left(1 + \dfrac{\mathrm{Re}_p^{2/3}}{6}\right) & (\mathrm{Re_p} \le 1000) \\ 0.424 & (\mathrm{Re_p} > 1000) \end{cases}$$

$$m_p \frac{du_p}{dt} = \frac{\pi}{8}\rho_g d_p^2 C_D \left|u_g - u_p\right|\left(u_g - u_p\right) + m_p g$$

(4) Calculate particle temperature (T_p) using Eq. (1).

(5) Calculate particle diameter (d_p) and Al diameter (d_{Al}).

$$d_p = \left[\frac{6}{\pi}\left(\frac{m_{Al,(s)}}{\rho_{Al}} + \frac{m_{Al,(l)}}{\rho_{Al}} + \frac{m_{mox}}{\rho_{mox}}\right)\right]^{1/3}$$

$$d_{Al} = \left[\frac{6}{\pi}\left(\frac{m_{Al,(s)}}{\rho_{Al}} + \frac{m_{Al,(l)}}{\rho_{Al}}\right)\right]^{1/3}$$

(6) If the particle temperature is lower than the melting temperature of aluminum, iterate from (1) to (5). Or not, calculate liquid aluminum production rate ($\dot{m}_{sl}$) and reduction rate ($\dot{m}_{ls}$) using Eq. (2) and (3), respectively.

(7) Iterate from (1) to (6) until the particle temperature reaches melting temperature of aluminum oxide.

(Procedure for QSC stage)

(1) Assume mass fraction of aluminum ($Y_{Al,s}^{guess}$) and mass ratio (f^{guess}).

(2) Calculate mass transfer number (B_{Al-ox}) using Eq. (7).

(3) Calculate mass fraction of species- (i) at the particle surface ($Y_{i,s}$) using Eq. (8).

(4) Calculate molar mass of mixture.

$$MW_{mix,s} = 1\Big/\left(\sum_i Y_i / MW_i\right)$$

(5) Calculate vapor pressure of aluminum near the surface using Antoine equation presented in NIST database.

(6) Calculate $Y_{Al,s}^{new}$ and f^{new}

$$Y_{Al,s}^{new} = \frac{p_{Al,vap}}{p_{amb}}\left(\frac{MW_{Al}}{MW_{mix}}\right)$$

$$f^{new} = \frac{Lh \cdot \left(Y_{Al,s}^{new} + Y_{ox,\infty}/\nu_{ox}\right)}{\left[c_{p,g}\left(T_\infty - T_p\right) - H_r\, Y_{ox,\infty}/\nu_{ox}\right]} + \frac{\left(1 - Y_{Al,s}^{new}\right)\left[H_r\left(Y_{ox,\infty}/\nu_{ox}\right) - c_{p,g}\left(T_\infty - T_p\right)\right]}{\left[c_{p,g}\left(T_\infty - T_p\right) - H_r\, Y_{ox,\infty}/\nu_{ox}\right]}$$

(7) Substitute $Y_{Al,s}^{new}$ (or f^{new}) for $Y_{Al,s}^{guess}$ (or f^{guess}), and then repeat from (2) to (6) until their differences are small enough.

(8) Calculate non-dimensional number (Re, Pr, Sc, Nu, Sh) with similar manner to the ignition stage.

(9) Calculate mass change rate $\dot{m}_p = \dot{m}_{tot,s}$, $\dot{m}_{Al,s}$ and $\dot{S}$.

$$\dot{m}_p = -\pi d_p \frac{\mu_g}{Sc_g} B \cdot Sh_p$$

$$\dot{m}_{Al,s} = \left(f + 1\right)\dot{m}_p \quad , \quad \dot{m}_{Al,s}'' - \dot{S}'' = \dot{m}_{tot,s}''$$

(10) Calculate ambient gas temperature ($T_{g,r}$) and penetrating heat ($\dot{Q}_L$) considering reaction effect using Eq. (11), (12) and (13), and then determine the effective latent heat of vaporization (Lh_{eff}).

(11) Calculate mass ratio f^{renew} containing energy transfer number as presented in Eq. (11).

$$f^{renew} = \frac{Lh_{eff}\left(Y_{Al,s}^{new} + Y_{ox,\infty}/\nu_{ox}\right)}{\left[c_{p,g}\left(T_\infty - T_p\right) - H_r\, Y_{ox,\infty}/\nu_{ox}\right]} + \frac{\left(1 - Y_{Al,s}^{new}\right)\left[H_r\left(Y_{ox,\infty}/\nu_{ox}\right) - c_{p,g}\left(T_\infty - T_p\right)\right]}{\left[c_{p,g}\left(T_\infty - T_p\right) - H_r\, Y_{ox,\infty}/\nu_{ox}\right]}$$

(12) Substitute f^{renew} for f^{new} , and then repeat from (2) to (11) until its difference are small enough.

(13) Calculate particle velocity with similar manner to the ignition stage.

(14) Calculate particle temperature (T_p).

$$\dot{Q}_L = m_p c_{p,p} \frac{dT_p}{dt}$$

(15) Calculate total particle mass (m_p), liquid aluminum mass ($m_{Al,s}$) and metal oxide mass (m_{mox}).

$$\dot{m}_p = \frac{dm_p}{dt} = -\pi d_p \frac{\mu_g}{Sc_g} B \cdot Sh_p$$

$$\frac{dm_{Al,s}}{dt} = \left(f + 1\right)\dot{m}_p \quad , \quad \frac{dm_{mox,s}}{dt} = -\dot{S}$$

(16) Calculate flame radius (r_f).

$$r_f = \left\{\frac{4\pi\mu_g}{Sc_g \dot{m}_p}\ln\left[\frac{Y_{ox,\infty}/\nu_{ox} + f + 1}{f + 1}\right]\right\}^{-1}$$

(17) Calculate flame temperature T_f using Eq. (14).

(18) Calculate diameter of aluminum (d_l) and particle (d_p).

$$d_{Al} = \left[\frac{6m_{Al}}{\rho_{Al}\pi}\right]^{1/3} \quad , \quad d_p = \left[6\left(\frac{m_{AL}}{\rho_{Al}} + \frac{m_p - m_{Al}}{\rho_{mox}}\right)\Big/\pi\right]^{1/3}$$

(19) Iterate from (1) to (18) until the liquid aluminum is exhausted.

Heesung Yang received B. S. (2003) degree from Yonsei University, Korea. He is a PhD candidate in Mechanical Engineering at Yonsei University. His current interests are vaporization, combustion of droplet and metallic particle combustion.

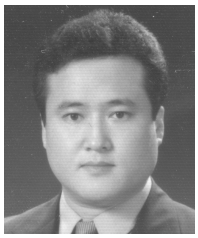

Woongsup Yoon received B. S. (1985) degree from Yonsei University, Korea. He received M. S. (1989) degree from Missouri-Rolla University and PhD (1992) degree from Alabama University, USA. Dr. Yoon is currently a Professor at the school of Mechanical Engineering at Yonsei University in Seoul, Korea.